Korean J. Chem. Eng., 33(2), 438-447 (2016)
DOI: 10.1007/s11814-015-0180-1

pISSN: 0256-1115
eISSN: 1975-7220

Dynamic modeling of fixed-bed adsorption of flue gas using a variable mass transfer model

Jehun Park and Jae W. Lee†

Department of Chemical and Biomolecular Engineering, Korea Advanced Institute of Science and Technology (KAIST), 291, Daehak-ro, Yuseong-gu, Daejeon 34141, Korea
(*Received 29 April 2015 • accepted 21 August 2015*)

Abstract−This study introduces a dynamic mass transfer model for the fixed-bed adsorption of a flue gas. The derivation of the variable mass transfer coefficient is based on pore diffusion theory and it is a function of effective porosity, temperature, and pressure as well as the adsorbate composition. Adsorption experiments were done at four different pressures (1.8, 5, 10 and 20 bars) and three different temperatures (30, 50 and 70 °C) with zeolite 13X as the adsorbent. To explain the equilibrium adsorption capacity, the Langmuir-Freundlich isotherm model was adopted, and the parameters of the isotherm equation were fitted to the experimental data for a wide range of pressures and temperatures. Then, dynamic simulations were performed using the system equations for material and energy balance with the equilibrium adsorption isotherm data. The optimal mass transfer and heat transfer coefficients were determined after iterative calculations. As a result, the dynamic variable mass transfer model can estimate the adsorption rate for a wide range of concentrations and precisely simulate the fixed-bed adsorption process of a flue gas mixture of carbon dioxide and nitrogen.

Keywords: CO_2 Capture, Dynamic Modeling, Fixed Bed Adsorption, Flue Gas, Variable Mass Transfer Coefficient

INTRODUCTION

An international consensus for reducing carbon dioxide (CO_2) emissions is spreading worldwide, and as a result, interest in carbon capture and storage (CCS) technologies has gained wide attention. CCS is a comprehensive term that includes CO_2 capture, conversion, transport and storage technologies. Among these, CO_2 capture is an older technology compared to other CCS technologies. With the currently available technology, the concentration of CO_2 in the atmosphere is controlled by separating CO_2 from its emission sources like power plants and transported to storage facilities for further use in the future. Still, CO_2 capture is a research field that is the most progressive among CCS technologies and further studies are constantly being done [1].

Several methods for CO_2 capture have been proposed, and the representative methods are as follows: 1) liquid absorption [2,3], 2) solid adsorption [2-4] and 3) hydrate-based crystallization [5,6] The absorption technology normally uses liquid solvents as well as a significant amount of energy for the heating, cooling, and recycling of the carrier solvent. For example, a plant designed to capture 1,000 tons/day of CO_2 using the absorption technology for coal-fired flue gases costs $29.50 (USD) per tonnage production of CO_2 [7]. To have economic potential, the cost should be half that of the reference plant for 1,000 tons/day by considering the cost of CO_2 transportation and storage. As an alternative, sorption technologies using adsorbents have been widely studied to reduce the energy consumption. Various types of processes using adsorption technologies have been considered, and most of them [8-13] deal with vacuum swing adsorption (VSA) because the adsorbate can be entirely removed from the bed at the desorption step. The pressure swing adsorption (PSA) process, which operates above atmospheric pressure, has also been investigated. Gomes and Yee [14] carried out PSA adsorption and desorption operations at 3 and 1 bar, respectively. Ko et al. [15] investigated the optimization of the PSA process with a feed pressure of 2.56 bars and a purge pressure of 1.1 bars. Taking into consideration the CO_2 compression process after the capture process in CCS, the PSA process with a higher desorption pressure is operationally better than the VSA process.

Many studies on adsorbents for CCS have focused on the CO_2 equilibrium adsorption capacity and the selectivity of the equilibrium adsorbed amount of CO_2 compared to other gases contained in flue gases. Chue et al. [9] provided parameters for the Langmuir isotherm that were fitted to the equilibrium adsorbed amount of pure CO_2 and N_2 measured at different temperatures and at a low pressure range below 1.1 bars. Zhang et al. [16] studied the equilibrium adsorption capacity of CO_2 and N_2, respectively. Using the Langmuir-isotherm model, parameters were fitted to experimental results measured at high pressures up to 30 bars. Siriwardane et al. [17] researched the equilibrium adsorption capacity of CO_2, N_2 and H_2 on zeolites and AC at 25 °C. When the results of the aforementioned studies are summarized, zeolites including 13X have higher adsorption capacities for CO_2 than that of AC and better equilibrium selectivity in adsorbing CO_2 over N_2. Cavenati et al. [18] focused on adsorption equilibrium studies of CH_4, CO_2 and N_2 on 13X at high pressure conditions (up to 50 bars). Using Toth and multisite Langmuir isotherm models, they obtained the model parameters

†To whom correspondence should be addressed.
E-mail: jaewlee@kaist.ac.kr

by utilizing the experimental data for a wide range of pressures.

However, the adsorption process like the PSA method is not an equilibrium process but a rate-based process. To evaluate the adsorption process, not only the maximum equilibrium adsorption capacity on an adsorbent but also the rate of adsorption must be considered. In modeling of the adsorption rate, using a linear driving force (LDF) approximation is common, and the rate is dependent on the mass transfer coefficient and equilibrium adsorption amount. Combining material and energy balances, an equilibrium isotherm model can be used to build a dynamic model. The mass transfer coefficient is an important parameter in the dynamic model of adsorption. Some studies were able to obtain the optimal mass transfer coefficient after iterative simulations [8,9,19]. Ko et al. [15] and Kim et al. [20] calculated an effective mass transfer coefficient with Glueckauf's expression. Farooq and Ruthven [21] proposed an equation to obtain a mass transfer coefficient, and the equation considers macropores, micropores, and film resistances to mass transfer. Dantas [22,23] used this equation in the modeling of gas adsorption on adsorbents in several studies. Although the mass transfer coefficient should not be considered as a constant in view of the pore diffusion theory, these studies have used a fixed value for the mass transfer coefficient.

In this study, we investigated the adsorption of a N_2 and CO_2 mixture on 13X in a fixed-bed column at temperatures ranging from 303 to 343 K and at elevated pressures between 1.8 and 20 bars. We propose a variable mass transfer model based on the pore diffusion theory, and evaluated the variable mass transfer coefficient based on changes in the operation parameters of temperature, pressure and adsorbate composition. To find the optimal mass and heat transfer coefficients, numerous dynamic simulations were performed iteratively. This study demonstrates the first attempt to introduce the dynamic mass transfer coefficient of an adsorbate to precisely simulate the mass transfer rate between gas and solid phases.

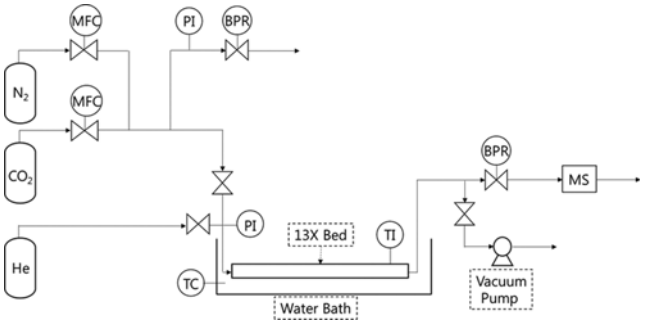

Fig. 1. Experimental system.

EXPERIMENTAL SECTION

1. Experimental Setup

Zeolite 13X (Sigma Aldrich) was used as an adsorbent and packed into a column. A schematic of experimental set-up is shown in Fig. 1. The column was installed in a water bath to maintain a constant temperature. Model parameters such as the dimension of the column, the physical properties of the adsorption material, the thermodynamic fluid properties and the adsorption properties are specified in Table 1. A mass flow controller (MFC Korea, Korea) was installed to control the gas flow from each gas cylinder. To control the pressure of the gas feed before the feed valve was released, a back pressure regulator (BPR) (Hiflux, Korea) was installed between the gas cylinder and the packed bed. The pressure of the fixed bed was maintained by another BPR (Swagelok, USA) mounted downstream of the column. The temperature indicator of the bed was positioned at the end of the bed, and a mass spectrometer (Pfeiffer Vacuum Schweiz AG, Switzerland) was mounted downstream of the column. In other words, the dynamic changes of the bed end temperature and the outlet gas composition were monitored while the system was in operation.

Table 1. Basic information of experiments and simulations

	Symbol	Unit	Value	Origin
Column length	L	m	0.263	Equipment
Column outer diameter	D_O	m	1.27×10^{-2}	Equipment
Column wall thickness	W_r	m	8.9×10^{-4}	Equipment
Density of bulk bed	ρ_s	kg/m^3	588	Measured
Radius of particle	R_p	m	2.6×10^{-3}	Measured
Interparticle porosity	ε_I	-	0.486	Calculated
Intraparticle porosity	ε_p	-	0.37	[22]
Density of particle	ρ_p	kg/m^3	1280	[22]
Heat capacity of particle	C_{ps}	kJ/kg·K	0.92	[8], [22]
Thermal conductivity of tube wall	k_w	kW/m·K	1.62×10^{-2}	Manufacturer
Heat capacity of tube wall	C_{pw}	kJ/kg·K	0.44	[22]
Density of tube wall	ρ_w	kg/m^3	7800	Manufacturer
Heat of adsorption of CO_2	$-\Delta H_{CO_2}$	kJ/mol	37.2	[18]
Heat of adsorption of N_2	$-\Delta H_{N_2}$	kJ/mol	12.8	[18]
Thermal conductivity of fluid gas	k_g	kW/m·K	2.5×10^{-5}	Calculated from Aspen plus
Thermal conductivity of 13X	k_s	kW/m·K	3.6×10^{-4}	[34]
Changes in gas composition according to partial pressure changes	$\partial c_i/\partial p_i$	mol/m^3·bar	38	Calculated from Aspen plus

2. Experimental Procedure

The column was first heated to 110 °C, and desorption was performed under a vacuum (below 0.01 bars). Most of the gases adsorbed on the 13X were desorbed at this point. Furthermore, the column was filled with helium (He) to provide an inert condition. Before opening the feed valve, each gas flow was turned on and held until the flow reached its set value of 160 and 40 sccm for N_2 and CO_2, respectively. Additionally, the pressure of the gas feed section was regulated to be the same as the column pressure with the BPR. Thus, the pressure at both sides was confirmed to be the same and stably maintained throughout the experiment. Experiments were performed at four different pressures: 1.8, 5, 10, and 20 bars. When the temperature of the water bath reached a preset value, the adsorption was started by opening the feed valve. At the same time, the He feed valve and BPR positioned in the gas feed section were closed. Each experiment was conducted at 303, 323 and 343 K. Dynamic changes in the temperature and outlet gas compositions were monitored.

MODELING

A commercial simulator, Aspen Adsorption™, was used for the numerical modeling of the experiment data. The material and energy balances used in this study are presented below, and these are applicable to both general adsorbents and adsorbates, and the general adsorption process. This section also elucidates the derivation of the dynamic mass transfer coefficient model with the estimation of the inner and outer heat transfer coefficients.

1. Material Balance

The overall material balance of the gas phase and the material balances of each component are described in Eqs. (1) and (2), respectively. The first term in Eq. (2) describes the convective mass transfer of each gas used as an adsorbate. The second term accounts for the accumulation of the adsorbate in the pores, and the third term represents the mass transfer of the adsorbate between the gas and solid phases.

$$\frac{\partial(v_g\rho_g)}{\partial z}+\rho_s\Sigma_i\frac{\partial q_i}{\partial t}=0 \tag{1}$$

$$\frac{\partial(v_g c_i)}{\partial z}+\varepsilon_I\frac{\partial c_i}{\partial t}+J_i=0 \tag{2}$$

where v_g and ρ_g are the velocity and density of the gas, respectively; ρ_s is the bulk density of a sorbent, and q_i is the adsorbed amount of component i; c_i is the molar concentration of component i in the gas phase; ε_I is the porosity, and J_i is the mass transfer rate of component i. To calculate the mass transfer between the gas and solid phases, the following LDF (linear driving force) approximation in Eq. (3) is used which again shows the mass transfer between the gas and solid phases at the adsorbate.

$$J_i=\rho_s\frac{\partial q_i}{\partial t}=\rho_s k_i(q_i^*-q_i) \tag{3}$$

Here, k_{CO_2} is considered as a function of the pressure, temperature and concentration of the adsorbate whereas in other studies, k_i had been assumed as a constant value [8,9,15,19-23].

2. Energy Balance

For the energy balance, axial and radial thermal conductions were disregarded because heat transfer by conduction through the gas phase is much smaller than the heat transfer by convection. By assuming that the heat transfer between solid and gas phases is fast (T_g=T_s), the energy balance at the inner tube can be derived as in Eq. (4):

$$C_{vg}v_g\rho_g\frac{\partial T_g}{\partial z}+(\rho_s C_{ps}+\varepsilon_B C_{vg}\rho_g)\frac{\partial T_g}{\partial t}+P\frac{\partial v_g}{\partial z}+\rho_s\Sigma_i\left(\Delta H_i\frac{\partial q_i}{\partial t}\right)+\frac{4H_I}{D_I}(T_g-T_w)=0 \tag{4}$$

where C_{vg} is the specific heat capacity of the gas phase at a constant volume; C_{ps} is the specific heat capacity of the adsorbent; P is the total pressure of this system; T_g is the temperature of the gas phase, respectively; ΔH_i is the heat of adsorption of component i; H_I is the heat transfer coefficient between the gas phase and the wall, and D_I is the inner diameter of bed.

Next, the energy balance at the wall is expressed in Eq. (5), and the equation considers axial conduction, heat accumulation, heat transfer from the gas to the wall and from the wall to the cooling agent as follows:

$$-k_w\frac{\partial^2 T_w}{\partial z^2}+\rho_w C_{pw}\frac{\partial T_w}{\partial t}-H_I\frac{4D_I^2}{D_O^2-D_I^2}(T_g-T_w)+H_O\frac{4D_O^2}{D_O^2-D_I^2}(T_w-T_{amb})=0 \tag{5}$$

where k_w is the thermal conductivity of the wall; H_I and H_O are the inner and outer heat transfer coefficients; T_w is the wall temperature; T_{amb} is the ambient temperature; W_r is the width of the column wall, and D_O is the outer diameter of bed.

The pressure drop through the bed originates from the Ergun equation [24]. The Ergun equation combines the Carman-Kozeny equation for the laminar flow and the Burke-Plummer equation for the turbulent flow. Consequently, the modified Ergun equation is appropriate for both the laminar and turbulent flows. Additionally, it is the most accepted equation for calculating the pressure drop [25].

$$\frac{\partial P}{\partial z}=-\left(\frac{1.5\times10^{-3}(1-\varepsilon_I)^2}{(2r_p\psi)^2\varepsilon_I^3}\mu v_g+1.75\times10^{-5}M\rho_g\frac{(1-\varepsilon_I)}{2r_p\psi\varepsilon_I^3}v_g^2\right) \tag{6}$$

Here, r_p and ψ are the radius and shape factor of the sorbent particle, and M is the molecular weight of the gas, respectively.

3. Adsorption Isotherm

According to Dantas et al. [22], the active sites for N_2 and CO_2 on 13X are independent of each other. In addition, the pure gas Toth isotherm has good performance in predicting the amount of CO_2 adsorption, which is comparable to the multicomponent Toth isotherm. Thus, we used several isotherms for the pure gas type to calculate the adsorption amount of CO_2 and N_2. The Langmuir model [26] is the most well-known and commonly used as an isotherm model. Thus, the following modified Langmuir isotherm was considered.

$$q_i^*=\frac{q_{si}K_i q_i}{1+K_i q_i} \tag{7}$$

Each parameter for the isotherm model is a function of the temperature and can be obtained as follows.

$$q_{si} = \omega_i \exp\left(\frac{-\theta_i}{RT}\right) \quad (8)$$

$$K_i = \Omega_i \exp\left(\frac{-\Theta_i}{RT}\right) \quad (9)$$

These parameters have the same forms for the Freundlich isotherm model and the Langmuir-Freundlich isotherm model. The Freundlich isotherm [27] is frequently used to show the adsorption characteristics of a heterogeneous surface, and the general form of the Freundlich isotherm is written in Eq. (10).

$$q_i^* = K_i q_i^n \quad (10)$$

The Langmuir-Freundlich isotherm (Eq. (11), [28,29]) is a versatile isotherm equation.

$$q_i^* = \frac{q_{si} K_i P_i^n}{1 + K_i P_i^n} \quad (11)$$

When the outlet gas concentrations reach the original feed compositions, the system is assumed to reach the equilibrium state. The equilibrium adsorption amount is calculated from the amount of adsorbed gas until reaching the equilibrium state. Table 2 shows the amount of each gas adsorbed at equilibrium under the different temperature and pressure conditions. According to Cavenati et al. [18], when the partial pressure of CO_2 is low, the equilibrium amount of CO_2 adsorbed on 13X changes rapidly according to the partial pressure of CO_2. Instead, when the partial pressure of CO_2 is high, it increases slowly and does not converge toward a specific value. The results (Table 2) show a trend similar to previous results [18]. The parameters for each isotherm model obtained from the equilibrium adsorption amounts are listed in Table 3. By comparing several isotherm models, the best isotherm model is chosen to describe the equilibrium adsorbed amount (Figs. 2-4). First, the Langmuir model is inadaptable to an adsorbent like 13X which has heterogeneous sites. The derivative of the Freundlich isotherm is $(\partial q^*/\partial p_i) = K_i n(1/P_i^{(1-n)})$, and this term is inversely proportional to

Table 2. Adsorbed amount of CO_2 and N_2 on 13X at equilibrium

Pressure (bars)	Temperature (K)	p_{CO_2} (bars)	$q^*_{CO_2}$ (mol/kg)	p_{N_2} (bars)	$q^*_{N_2}$ (mol/kg)
1.8	303	0.37	3.12	1.43	0.41
	323	0.37	2.52	1.43	0.37
	343	0.37	1.79	1.43	0.21
5	303	1.04	3.85	3.96	0.80
	323	1.04	3.23	3.96	0.66
	343	1.04	2.59	3.96	0.53
10	303	2.08	4.42	7.92	1.36
	323	2.08	3.83	7.92	1.12
	343	2.08	3.29	7.92	0.92
20	303	4.17	4.98	15.83	2.11
	323	4.17	4.52	15.83	1.87
	343	4.17	3.89	15.83	1.62

Table 3. Isotherm parameters of CO_2 and N_2 adsorption on 13X

		CO_2	N_2
Modified Langmuir (Eq. (7)-(9))	ω_i [mol/kg]	1.414	0.358
	$-\theta_i$ [J/mol]	3225	6727
	Ω_i [1/bar]	2.14×10^{-3}	4.5×10^{-2}
	$-\Theta_i$ [J/mol]	18933	0
Modified Freundlich (Eq. (9), (10))	Ω_i [mol/kg·bar]	0.239	1.34×10^{-2}
	$-\Theta_i$ [J/mol]	6915	8364
	n [-]	0.237	0.625
Langmuir-Freundlich (Eq. (8), (9), (11))	ω_i [mol/kg]	6.54	8.73
	$-\theta_i$ [J/mol]	0	0
	Ω_i [1/bar]	1.72×10^{-3}	1.2×10^{-3}
	$-\Theta_i$ [J/mol]	17029	8283
	n [-]	0.534	0.838

increases in P_i. However, the CO_2 adsorption capacity of 13X does not increase as fast as the estimation of the Freundlich model. In

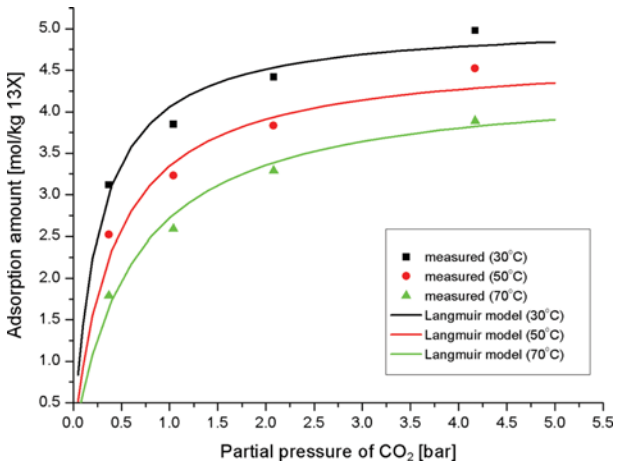

Fig. 2. Amount of CO_2 adsorption: comparison between the modified Langmuir model prediction and experimental data.

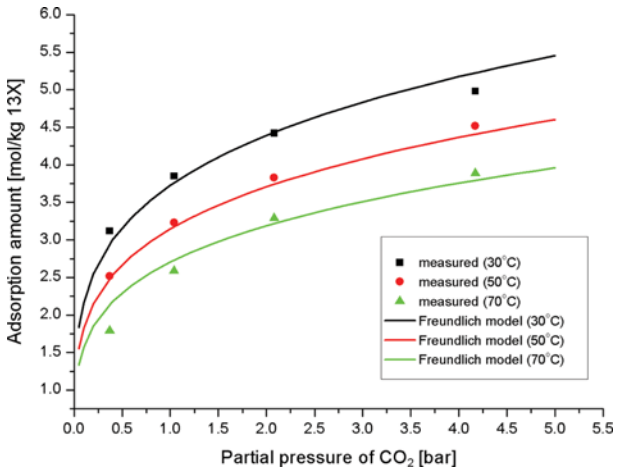

Fig. 3. Amount of CO_2 adsorption: comparison between the modified Freundlich model prediction and experimental data.

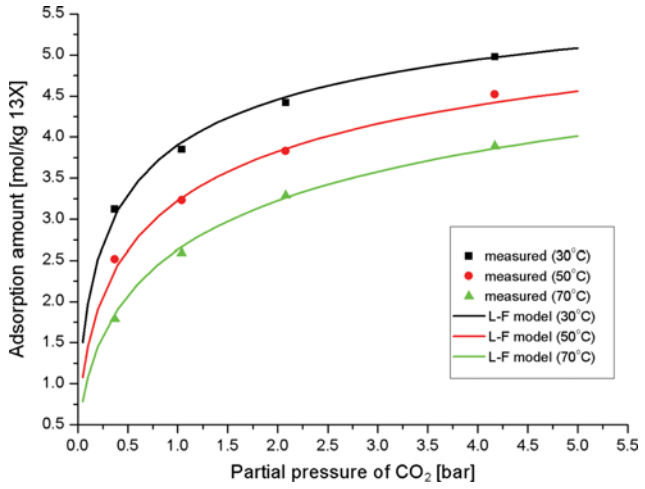

Fig. 4. Amount of CO_2 adsorption: comparison between the Langmuir-Freundlich model prediction and experimental data.

contrast, the Langmuir-Freundlich isotherm matches well the experimental outcome, which is better than that of other models. Thus, we mainly used the Langmuir-Freundlich isotherm model and its parameters for the dynamic modeling of the fixed-bed adsorption.

4. Dynamic Mass Transfer Coefficient

Several previous studies [15,20-23] have reported that the mass transfer coefficient varies depending on the final steady state conditions of the temperature, pressure and adsorbate concentration. As the adsorption experiment progresses, the temperature and pressure and especially the concentration of the adsorbates change dynamically. Thus, dynamically variable mass transfer coefficients should be considered. Because the mass transfer rate is determined by diffusion at the pore, Tien [30] derived the mass transfer coefficient (k_i) as follows:

$$k_i = \frac{15\varepsilon_p}{R_p^2}\frac{D_M}{\tau f'(c_i)\rho_p} \tag{12}$$

where R_p is a particle radius; ε_p is the intraparticle porosity; τ is the tortuosity; D_M is the molecular diffusivity that is calculated by the Chapman-Enskog equation [25], and ρ_p is the particle density. $f'(c_i)$ is a differential term of the isotherm for the gas concentration and this term is shown in Eq. (13) if the Langmuir-Freundlich isotherm in Eq. (11) is used:

$$f'(c_i) = \frac{\partial q_i}{\partial p_i}\frac{\partial p_i}{\partial c_i} = \frac{nq_{si}K_iP_i^{(n-1)}}{(1+K_iP_i^n)^2}\frac{\partial p_i}{\partial c_i} \tag{13}$$

where $\partial c_i/\partial p_i$ is the gas composition change according to the partial pressure and can be assumed as a constant.

Next, the tortuosity also can be calculated by using Eq. (14) which is suggested by Barrande et al. [31]

$$\tau = 1 - 0.49\ln(\varepsilon_p) \tag{14}$$

Finally, the effective porosity ($\bar{\varepsilon}_p$) can be defined with Eq. (15) by introducing K_d which is the ratio between the total intraparticle porosity and the porosity actually penetrated by gas [32].

$$\bar{\varepsilon}_p = K_d\varepsilon_p \tag{15}$$

Using $\bar{\varepsilon}_p$ instead of ε_p in Eqs. (12) and (14) by considering the actual penetration of gas into the pores and inserting Eqs. (13)-(15) into Eq. (12) yield Eq. (16).

$$k_i = \frac{15}{R_p^2\{1-0.49\ln(K_d\varepsilon_p)\}}\frac{K_d\varepsilon_p}{\rho_p}\frac{D_M}{\{nq_{si}K_iP_i^{(n-1)}\}}\frac{(1+K_iP_i^n)^2}{\partial p_i}\frac{\partial c_i}{} \tag{16}$$

The functional form of the mass transfer coefficient in Eq. (16) is used to calculate the mass balance (Eqs. (1)-(3)) for the following dynamic simulation.

5. Inner Heat Transfer Coefficient

Yagi and Kunii [33] studied heat transfer in a fixed bed using two terms for heat transfer due to the gas flow. The expression is available in Eq. (17) [34].

$$H_I = H_I^o + \frac{\alpha_w k_g}{2R_p}\mathrm{PrRe}_p = \frac{k_{ew}^o}{R_p} + \alpha_w(C_{pg}\rho_g v_g) \tag{17}$$

where k_{ew}^o is the effective thermal conductivity of a thin layer bed near the wall surface; α_w is the constant for the heat transfer by forced convection; Pr is the Prandtl number, and Re_p is the particle Reynolds number.

The value of α_w differs in many studies; however, a reasonable value is about 0.05 [34]. The product of Pr and Re_p is smaller than 10 for this system. Thus, the second term of Eq. (17) is much smaller than the first term that can be ignored. The inner heat transfer is only affected by the conduction of gas and solid near the wall because the gas velocity is very low, and the particle size is very small. k_{ew}^o can be represented by Eq. (18) as follows:

$$k_{ew}^o = \varepsilon_w k_g + (1-\varepsilon_w)k_s\frac{1}{\phi_w\left(\frac{k_s}{k_g}\right)+\frac{1}{3}} \tag{18}$$

where ε_w is the mean void fraction of this wall layer; k_g is the thermal conductivity of the gas fluid; k_s is the thermal conductivity of the adsorbent, and ϕ_w is the ratio of the effective thickness of the gas film around a contact between the particle and the surface.

Kunii and Smith [35] calculated ϕ_w depending on k_s/k_g, and the proper value for this study is 0.2. H_I can be assumed as a constant because k_g is almost constant during the experiments, and the gas velocity cannot affect the heat transfer. Although ε_w has an unknown value, the initial H_I can be estimated by assuming $\varepsilon_w=\varepsilon_t$. Then, the initial guess of H_I is 53 W/m^2·K for the dynamic simulations. After that, fitting to the experimental data was performed with varying values of H_I.

6. Outer Heat Transfer Coefficient

Because there is no introduction of forced convection for cooling, we used Eq. (19) to obtain the outer heat transfer coefficient due to natural convection [36] as follows:

$$H_O = 0.53\frac{k_c}{D_O}(\mathrm{Gr}\cdot\mathrm{Pr})^{0.25} \qquad (\text{Range: } 10^3 < \mathrm{Gr}\cdot\mathrm{Pr} < 10^9) \tag{19}$$

where k_c is the thermal conductivity of the cooling agent; Gr is the Grashof number, and Pr is the Prandtl number.

Fig. 5 shows the calculation result of H_O according to the temperature difference between two fluids of adsorbate gas and the cooling agent. H_O is approximately 900 W/m^{2}K when water is used

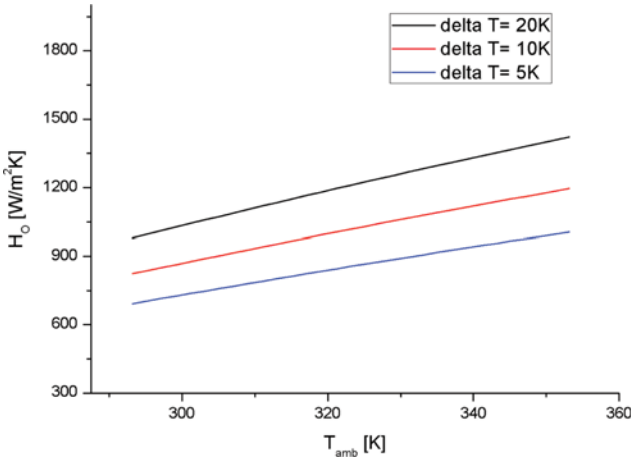

Fig. 5. Estimation of outer heat transfer coefficient using water as a cooling agent.

as a cooling agent. Therefore, when water is the cooling agent, the overall heat transfer coefficient is determined by the inner heat transfer coefficient because H_O is much bigger than H_I.

7. Summary of the Modeling Procedure

The modeling procedure is shown in Fig. 6. First, the optimal adsorption isotherm model was selected, and the parameters of the isotherm model were calculated. Then, the proper balance for the mass and energy was established. The conditions of the bed experiments, the parameters of the isotherm model and the mass and heat transfer coefficients were entered into the model. The initial mass transfer coefficient and heat transfer coefficient were calculated using Eqs. (16)-(19). After the basic model was set up, iterative dynamic simulations were performed to obtain the optimal mass and heat transfer coefficient. The values of K_d and heat transfer coefficient were changed until simulation results matched the measured outlet composition and temperature profile. The mass transfer coefficient has to fit in advance because it changes more sensitively than the heat transfer coefficient. Therefore, there was no significant change in the calculation results of the outlet composition caused by the change in temperature or change in the heat transfer coefficient. Finally, a model was obtained with an optimal K_d for the dynamic mass transfer coefficient and heat transfer coefficients.

LIMITATION OF A CONSTANT MASS TRANSFER COEFFICIENT (k_i)

The normalized outlet gas composition was measured and plot-

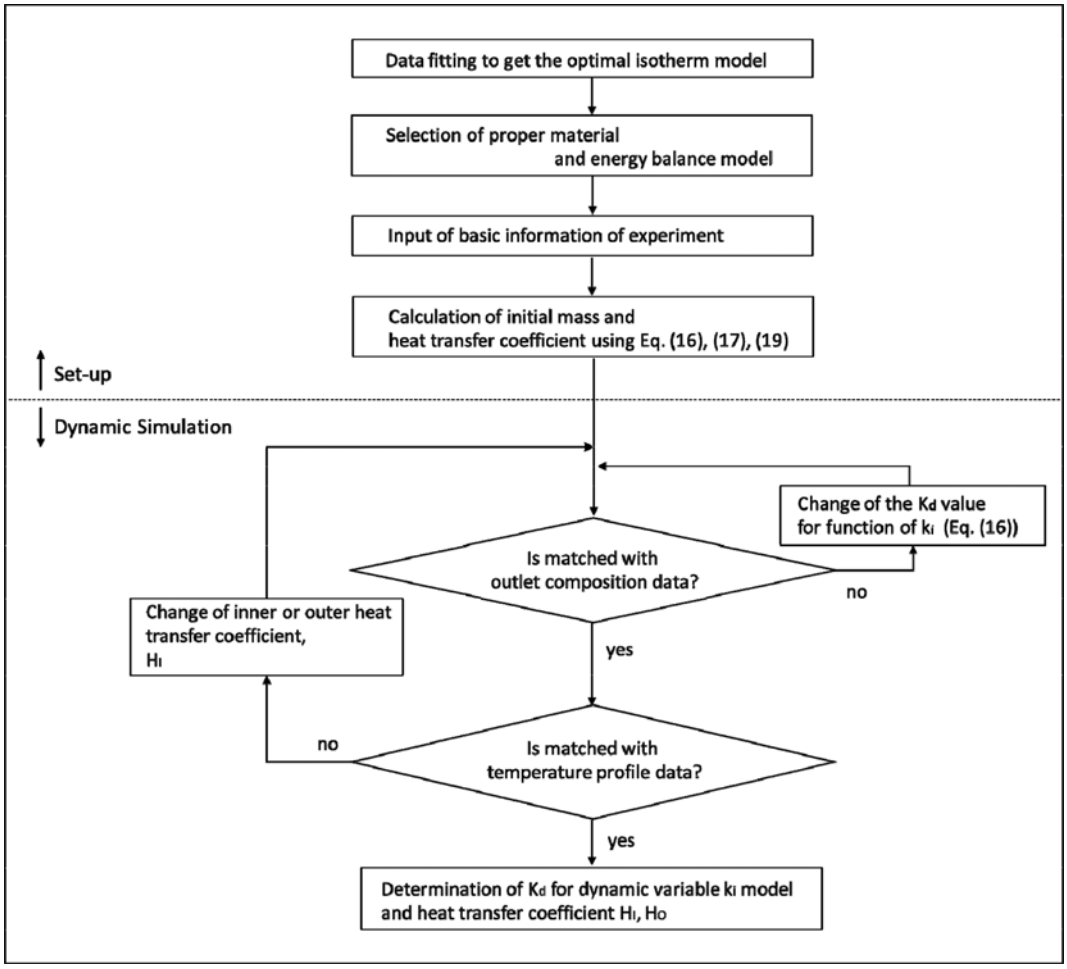

Fig. 6. Modeling procedure.

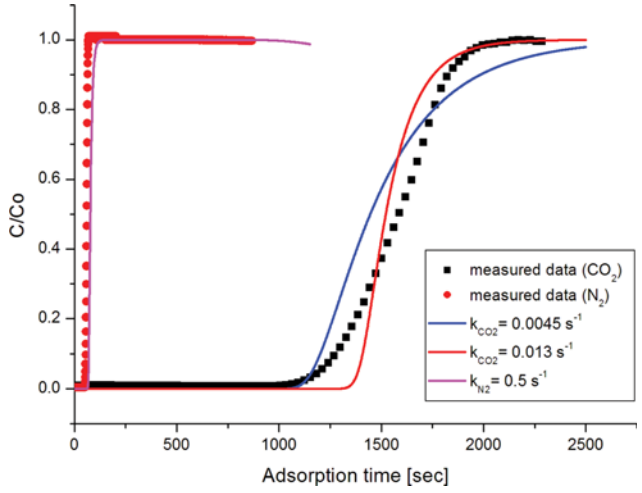

Fig. 7. Comparison of measured data and simulation results with constant mass transfer coefficient (k_{CO_2}=0.0045 s^{-1} and 0.013 s^{-1}) at 1.8 bars and 323 K.

ted against time. The normalized composition was defined as the outlet composition divided by the initial gas composition. A N_2 peak was observed earlier than the CO_2 peak, and the slope of the N_2 outlet composition over time was significantly larger than that of CO_2. That is, the N_2 adsorption capacity on 13X is extremely small, and the mass transfer coefficient of N_2 is much bigger than that of CO_2. Fig. 7 shows that CO_2 is detected earlier in the experiment than in the simulation when a constant mass transfer coefficient is used (k_{CO_2}=0.013 s^{-1}). The detection time of CO_2 from the simulation result with k_{CO_2}=0.0045 s^{-1} yielded a result similar to the experiment result. However, the simulation result for the high CO_2 concentration range did not match with the experiment result. Therefore, when the CO_2 concentration is low, the mass transfer coefficient is small and a large amount of CO_2 passes through the bed without adsorption. Additionally, as the CO_2 concentration increases, the mass transfer coefficient also increases in the real measurements. Next, the most proper mass transfer coefficient of each experiment was investigated depending on the pressure change. The outlet composition from the bed was measured at pressures of 1.8, 5, 10 and 20 bars, and constant mass transfer coefficients with values of 0.013, 0.02, 0.04, and 0.4 sec^{-1}, respectively, were used to fit the measured values in Fig. 8. The data confirmed that the mass transfer coefficients increase as the total pressure increases. Because the purpose of the model is to provide a prediction capability for unmeasurable conditions, the mass transfer coefficient should be a variable with high reliability without additional experiments. Additionally, as confirmed in Fig. 8, there was a significant difference in the initial CO_2 detection times among the four different cases. Therefore, when these constant mass transfer coefficients are used, it may be possible to simulate the overall behavior of a gas; however, they cause tremendous errors in the calculated adsorption rate when the CO_2 concentration (partial pressure) is low.

DYNAMIC SIMULATION RESULTS FOR THE VARIABLE k_i

1. Effect of Pressure

When the partial pressure of the adsorbate increases, $f'(c_i)$ decreases, and hence the mass transfer coefficient (k_i in Eqs. (12) and (16)) becomes larger. Therefore, at the beginning of the adsorption step, k_i has a small value because the concentration of the adsorbate is low. However, as the adsorption progresses, the value of k_i increases in proportion to the adsorbate concentration. Then, it can overcome the deviation caused by using a constant k_i because

Table 4. Optimal K_d and $\bar{\varepsilon}_p$ depending on pressure and heat transfer coefficient

Pressure	1.8 bar	5 bar	10 bar	20 bar
K_d (initial K_d)	0.1 (1.0)	0.105 (1.0)	0.28 (1.0)	0.55 (1.0)
$\bar{\varepsilon}_p$ (initial $\bar{\varepsilon}_p$)	0.037 (0.37)	0.038 (0.37)	0.105 (0.37)	0.204 (0.37)
H_I (initial H_I)	80 W/m^2·K (53 W/m^2·K)			

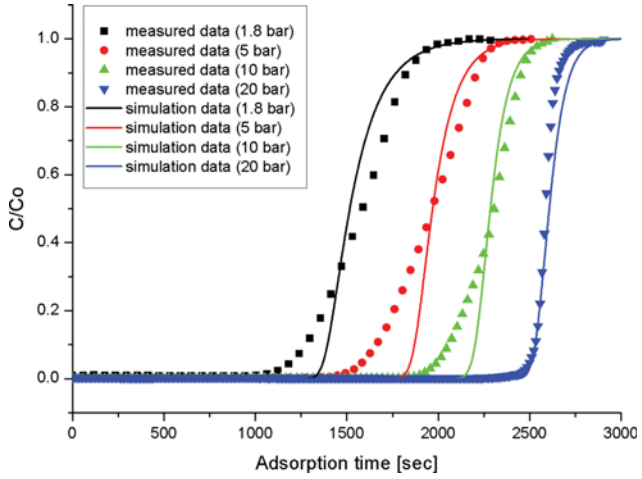

Fig. 8. CO_2 breakthrough curves depending on the pressure (k_{CO_2}= 0.013 sec^{-1} at 1.8 bars, 0.02 sec^{-1} at 5 bars, 0.04 sec^{-1} at 10 bars, and 0.4 sec^{-1} at 20 bars, ambient temperature: 323 K).

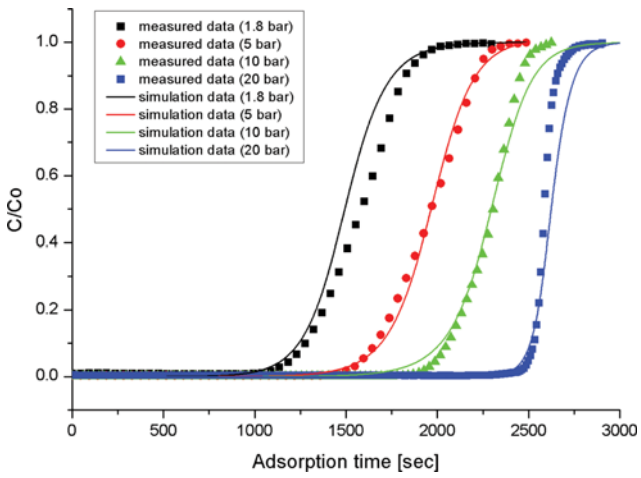

Fig. 9. CO_2 breakthrough curves depending on the pressure. Simulation data is calculated using the variable k_i (ambient temperature: 323 K).

the variable mass transfer coefficient can precisely simulate the breakthrough curves for a wide range of concentrations. As mentioned in the modeling procedure of Fig. 6, several optimal values of K_d were obtained that make the simulation results match well with the experiment results. The optimal K_d values are listed in Table 4 with respect to the pressure and K_d increases in proportion to the pressure. It can be surmised that the increased pressure causes an increase in the availability of pores for the penetration of the adsorbate gas. Fig. 9 shows a comparison between the outlet compositions calculated with the variable k_i and the experiment results. The variable k_i describes the overall outlet compositions more precisely than does the constant k_i shown in Fig. 8. The initial values of H_I and H_O are obtained from Eqs. (17) and (19). When water is used as a cooling agent, the overall heat transfer coefficient is determined by H_I alone because H_I is much smaller than H_O. H_I is fitted to find an optimal value which can precisely match between the calculated and measured temperature profiles. As a result, the optimal value for H_I is 80 W/m^2·K and Fig. 10 shows a comparison between the measured results and the calculated temperature profiles.

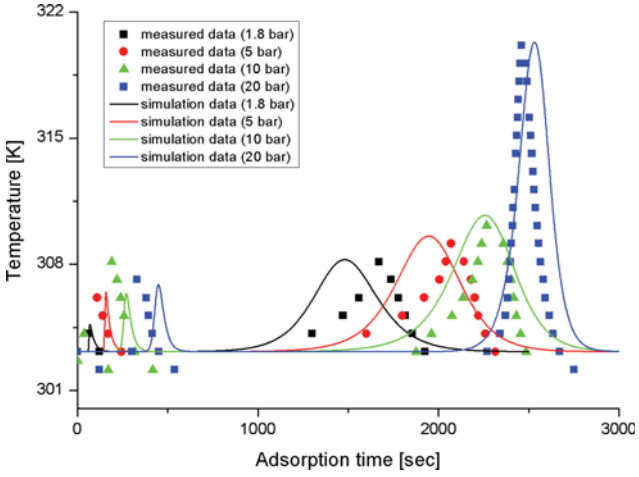

Fig. 10. Comparison of temperature profiles depending on the pressure. Simulation data is calculated using the variable k_i (cooling agent: water, ambient temperature: 323 K).

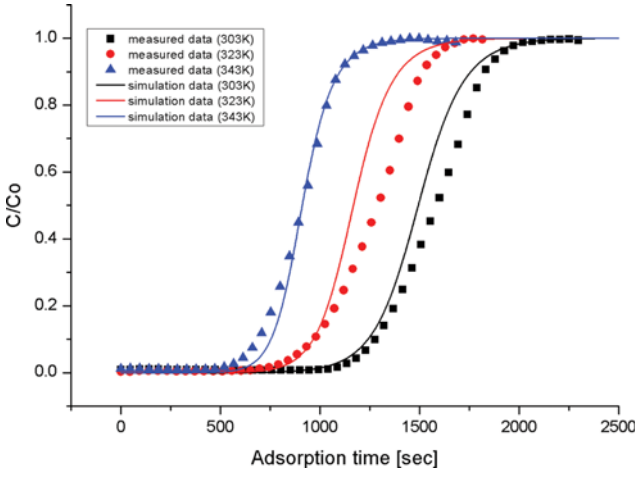

Fig. 11. CO_2 breakthrough curves depending on the temperature. Simulation data is calculated using the variable k_i (pressure: 1.8 bar).

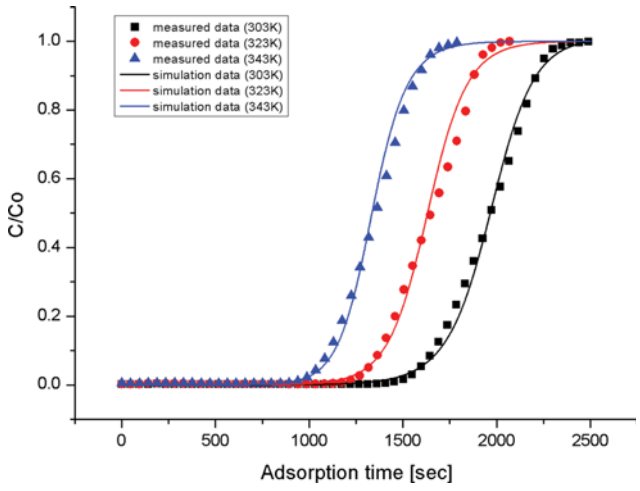

Fig. 12. CO_2 breakthrough curves depending on the temperature. Simulation data is calculated using the variable k_i (pressure: 5 bar).

2. Effect of Temperature

Fig. 11 shows a comparison between the calculated breakthrough curves at 1.8 bars and the measured profiles at three different temperatures. The slope becomes gradually steep at the initial stage of increasing the outlet concentration as the temperature increases. The reason is that the molecular diffusion (D_M) increases proportionally to the temperature and the mass transfer coefficient increases as well. Fig. 12 shows both the simulation results and experimental data for the outlet compositions at 5 bars. However, the slope change is negligible at the initial stage of increasing the outlet concentration with respect to temperature changes. This means that the initial change in the slope is less sensitive to temperature changes once the pressure moves up to 5 bars. The mass transfer coefficient becomes larger at 5 bars and the temperature change at this pressure does not additionally contribute to improving the mass transfer.

CONCLUSIONS

Zeolite 13X was packed in a fixed bed and the adsorption of a CO_2/N_2 flue gas mixture was analyzed with equilibrium isotherms and dynamic modeling for both mass and heat transfer. The breakthrough experiments were performed at different temperatures (303, 323 and 343 K) and pressures (1.8, 5, 10 and 20 bars). To describe the equilibrium adsorption amount, the Langmuir-Freundlich isotherm model was chosen as the best isotherm model, and the parameters of the isotherm model for CO_2 and N_2 were obtained. The mass transfer coefficient was introduced as a function of the effective intraparticle porosity, pressure, temperature and adsorbate concentration. The fraction of effective intraparticle porosity to total intraparticle porosity (K_d) was used to indicate pore accessibility by gas molecules when proposing the concept of the variable mass transfer coefficient. The proposed variable mass transfer model can provide an accurate estimate of the mass transfer rate for a wide range of adsorbate compositions.

ACKNOWLEDGEMENTS

The authors are grateful for the financial support from the Korea CCS R & D Center and funded by the Ministry of Science, ICT, and Future Planning (no. NRF-2014M1A8A1049297).

NOMENCLATURE

C_{ps} : specific heat capacity of the adsorbent [kJ/kg·K]
C_{pw} : specific heat capacity of the column wall [kJ/kg·K]
C_{vg} : specific heat capacity of the gas phase at a constant volume [kJ/mol·K]
c_i : molar concentration of component i [mol/m^3]
D_I : inner diameter of the tube [m]
D_M : binary molecular diffusivity [m^2/s]
D_O : outer diameter of the tube [m]
Gr : Grashof number $(=\frac{g\rho^2\beta\Delta T(D_O)^2}{\mu^2})$
H_I : heat transfer coefficient between the gas phase and wall [kW/m^2·K]
H_I^o : heat transfer coefficient near the wall by a stagnant flow [kW/m^2·K]
H_O : heat transfer coefficient between the wall and ambient [kW/m^2·K]
ΔH_i : heat of adsorption of component i [kJ/mol]
J_i : mass transfer rate of component I to adsorbent [mol/m^{3}bed·s]
k_c : thermal conductivity of the cooling agent [W/m·K]
K_d : fraction of intraparticle volume species that can penetrate pores
k_{ew}^o : effective thermal conductivity of a thin layer bed near the wall surface [W/m·K]
k_g : thermal conductivity of a fluid gas [W/m·K]
k_i : mass transfer coefficient of component i [1/s]
K_i : parameter of the adsorption isotherm model
k_w : thermal conductivity of the column wall [W/m·K]
k_s : thermal conductivity of the adsorbent [W/m·K]
L : length of the column [m]
n : heterogeneous index of the Freundlich isotherm model
P : total pressure [bars]
Pr : Prandtl number $(=\frac{\mu C_p}{k})$
Re_p : particle Reynolds number $(=\frac{2R_p v_g \rho_g}{\mu_g})$
q_i^* : amount of component i adsorbed at the equilibrium state [mol/kg]
q_i : real loading of component i at a specific time [mol/kg]
q_{si} : maximum capacity of Langmuir isotherm or Langmuir-Freundlich isotherm model [mol/kg]
R_p : particle radius [m]
t : time [s]
T_{amb} : ambient temperature [K]
T_g : gas phase temperature [K]
T_s : solid phase temperature [K]
T_w : wall temperature [K]
v_g : gas velocity [m/s]
W_r : width of the tube wall [m]
z : Axial co-ordinate [m]

Greek Letters

α_w : constant for heat transfer by forced convection [-]
ε_i : interparticle porosity [m^3 (interparticle void)/m^3 (bed)]
ε_p : intraparticle porosity [m^3 (intraparticle void)/m^3 (particle)]
$\bar{\varepsilon}_p$: effective intraparticle porosity [m^3 (intraparticle void)/m^3 (particle)]
ε_w : the mean void fraction of this wall layer [-]
θ : parameter for temperature dependent description of q_{si} [J/mol]
Θ : parameter for temperature dependent description of K_i [J/mol]
μ : dynamic viscosity [Pa·s]
ρ_g : molar gas phase density [mol/m^3]
ρ_p : particle density [kg/m^3]
ρ_s : bulk solid phase density [kg/m^3]
ρ_w : wall density [kg/m^3]
τ : tortuosity of a particle [-]
ϕ_w : ratio of the effective thickness of a gas film around a contact between the particle and the surface [-]
ψ : shape factor [-]
ω : parameter for temperature dependent description of q_{si} [mol/kg]
Ω : parameter for temperature dependent description of K_i [1/bar] or [mol/kg·bar]

REFERENCES

1. S. Park and T. Park, *J. KSME*, **47**(7), 11 (2007).
2. P. Folger, *Carbon Capture: A Technology Assessment*, CRS Report for Congress (2010).
3. C.-H. Yu, C.-H. Huang and C.-S. Tan, *Aerosol and Air Quality Research*, **12**, 745 (2012).
4. K. Kim, S. Yang, J. B. Lee, T. H. Eom, C. K. Ryu, H.-J. Lee, T.-S. Bae, Y.-B. Lee and S.-J. Lee, *Korean J. Chem. Eng.*, **32**(4), 677 (2015).
5. P. Linga, A. Adevemo and P. Englezos, *Environ. Sci. Technol.*, **42**, 315 (2008).
6. J. Zhang, P. Yedlapalli and J. W. Lee, *Chem. Eng. Sci.*, **64**, 4732 (2009).
7. D. G. Chapel, C. L. Mariz and J. Ernest, *Canadian Society of Chemical Engineers Annual Meeting*, October 4-6 (1999).
8. E. S. Kikkinides, R. T. Yang and S. H. Cho, *Ind. Eng. Chem. Res.*, **32**, 2714 (1993).
9. K. T. Chue, J. N. Kim, Y. J. Yoo, S. H. Cho and R. T. Yang, *Ind. Eng. Chem. Res.*, **34**, 591 (1995).
10. B.-K. Na, K.-K. Koo, H.-M. Eum, H. Lee and H. K. Song, *Korean J. Chem. Eng.*, **18**(2), 220 (2001).
11. W. Choi, T. Kwon, Y. Yeo, H. Lee, H. K. Song and B. Na, *Korean J. Chem. Eng.*, **20**(4), 617 (2003).
12. S. Cavenati, C. A. Grande and A. E. Rodrigues, *Chem. Eng. Sci.*, **61**, 3893 (2006).
13. C. Chou and C. Chen, *Sep. Purif. Technol.*, **39**, 51 (2004).
14. V. G. Gomes and K. W. K. Yee, *Sep. Purif. Technol.*, **28**, 161 (2002).
15. D. Ko, R. Siriwardane and L. T. Biegler, *Ind. Eng. Chem. Res.*, **42**, 339 (2003).
16. Z. Zhang, W. Zhang, X. Chen, Q. Xia and Z. Li, *Sep. Sci. Technol.*,

45(5), 710 (2010).
17. R. V. Siriwardane, M.-S. Shen, E. P. Fisher and J. A. Poston, *Energy Fuels*, **15**, 279 (2001).
18. S. Cavenati, C. A. Grande and A. E. Rodrigues, *J. Chem. Eng. Data*, **49**, 1095 (2004).
19. N. Casas, J. Schell, R. Pini and M. Mazzotti, *Adsorption*, **18**, 143 (2012).
20. J. Kim, K. Chue, K. Kim, S. Cho and J. Kim, *J. Chem. Eng. Japan*, **27**(1), 45 (1994).
21. S. Farooq and D. M. Ruthven, *Ind. Eng. Chem. Res.*, **29**, 1084 (1990).
22. T. L. P. Dantas, F. M. T. Luna, I. J. Silva Jr., A. E. B. Torres, D. C. S. de Azevedo, A. E. Rodrigues and R. F. P. M. Moreira, *Brazilian J. Chem. Eng.*, **28**(3), 533 (2011).
23. T. L. P. Dantas, F. M. T. Luna, I. J. Silva Jr., D. C. S. Azevedo, C. A. Grandec, A. E. Rodrigues and R. F. P. M. Moreira, *Chem. Eng. J.*, **169**, 11 (2011).
24. S. Ergun, *Chem. Eng. Prog.*, **48**, 89 (1952).
25. R. B. Bird, W. E. Stewart and E. N. Lightfoot, *Transport Phenomena*, Wiley, New York (1960).
26. I. Langmuir, *J. Am. Chem. Soc.*, **38**, 2221 (1916).
27. H. M. F. Freundlich, *J. Phys. Chem.*, **57**(A), 385 (1906).
28. R. Sips, *J. Chem. Phys.*, **16**(5), 490 (1948).
29. R. Sips, *J. Chem. Phys.*, **18**(8), 1024 (1950).
30. C. Tien, *Adsorption Calculations and Modeling*, Butterworth-Heinemann (1994).
31. M. Barrande, R. Bouchet and R. Denoyel, *Anal. Chem.*, **79**, 9115 (2007).
32. P. C. Wankat, *Rate-controlled Separations*, Elsevier (1990).
33. S. Yagi and D. Kunni, *AIChE J.*, **6**, 97 (1960).
34. D. Kunii and O. Levenspiel, *Fluidization Engineering 2nd*, Butterworth-Heinemann (1991).
35. D. Kunni and J. M. Smith, *AIChE J.*, **6**, 71 (1960).
36. C. O. Bennett and J. E. Myers, *Momentum, Heat and Mass Transfer 3rd*, McGraw-Hill (1982).